Supplementary Materials for

Unresolved endoplasmic reticulum stress engenders immune-resistant, latent pancreatic cancer metastases

Authors: Arnaud Pommier[1], Naishitha Anaparthy[1,4], Nicoletta Memos[1], Z Larkin Kelley[2], Alizée Gouronnec[1], Ran Yan[1], Cédric Auffray[5], Jean Albrengues[1], Mikala Egeblad[1], Christine A. Iacobuzio-Donahue[3], Scott K. Lyons[1], Douglas T. Fearon[1,2,6*]

Affiliations:
[1] Cold Spring Harbor Laboratory, Cold Spring Harbor, NY 11724, USA
[2] Weill Cornell Medicine, New York, NY 10065, USA
[3] Memorial Sloan Kettering Cancer Center, New York, NY 10065, USA
[4] Department of Molecular and Cellular Biology, Stony Brook University, NY 11794, USA
[5] Institut Cochin, Paris Descartes Université, CNRS UMR8104, INSERM U1016, 75014 Paris, France
[6] Cancer Research UK Cambridge Institute, University of Cambridge, Robinson Way, Cambridge CB2 0RE, UK

* Correspondence to:
Douglas T. Fearon
Cold Spring Harbor Laboratory
1 Bungtown Road
Cold Spring Harbor, NY 11724, USA
Phone: 516 367 5420
Email: dfearon@cshl.edu

This PDF file includes:

Supplementary tables

ID	Gender	Age at PDA diagnosis	Chemotherapy	Radiotherapy	Treatment for advanced disease	Outcome of treatment
PAM20	Female	81	Yes	Yes	5-FU	Progression
PAM57	Female	90	Yes	Yes	Gemcitabine	Progression
PAM15	Female	84	No	No		Progression
PAM51	Female	76	Yes	No	Gemcitabine	Progression
PAM43	Male	69	Yes	Yes	Gemcitabine + Erlotinib	Progression

Table S1: Clinicopathologic characteristics of patients

Figure number	Number of specimens (patients or mice)	Number of sections/specimen	Parameter assessed	% of positive DCCs
1 A	5	≥4	CK19	0
1 B	5	≥4	Ki67	0
1 C	5	≥4	MHCI	0
1 D	3	10	CK19	20
1 E	3	10	Ki67	0
1 F	3	10	MHCI	0
2 E	30	≥10	CK19	1.1
2 F	30	≥10	Ecad	0
2 G	5	≥5	Ki67	0
2 H	5	≥5	EdU	0
2 I	30	≥10	MHCI	0
2 J	30	≥10	CD3 contact	0.8
3 B	15	5	CK19	
3 C	15	5	MHCI	
4 G	5	5	CK19	
4 H	5	5	MHCI	
5 C	5	5	CHOP	100
5 D	3	5	CHOP	61.5
5 E	5	10	CHOP	57.9
6 A	30	5	pEIF2α	100
6 B	5	5	pEIF2α	84.6
6 C	30	5	pIRE1α	0
6 D	5	5	pIRE1α	0
S2 A	5	5	CD3 contact	53.8
S3 A	30	≥5	Desmin	0
S3 B	30	≥5	αSMA	0
S3 C	30	≥5	Snail1	0
S3 D	30	≥5	Slug	0
S4 C	5	5	CK19	0
S5 C	5	5	CK19	0
S6 A	5	10	CFSE	100
S6 B	5	10	EdU	4.4
S7 B	30	≥10	CD3 contact	0.8
S8 B	5	≥5	NKp46 contact	0
S9 A	30	5	CD45 contact	0
S9 B	30	5	F4/80 contact	0
S9 C	30	5	CD19 contact	0
S9 D	30	5	CD31 contact	0
S9 E	30	5	αSMA contact	0
S9 F	30	5	Ly6G contact	0
S9 G	3	2	CD45	
S9 H	3	2	F4/80	
S9 I	3	2	CD19	
S9 J	3	2	CD31	
S9 K	3	2	αSMA	
S9 L	3	2	Ly-6G	
S9 M	3	2	CD3	
S9 N	3	2	NKp46	
S15 F	5	≥5	MHCI	100

Table S2: Specimen, section numbers, parameter assessed and percentage of positive events among DCCs relating to figures.

Supplementary figures

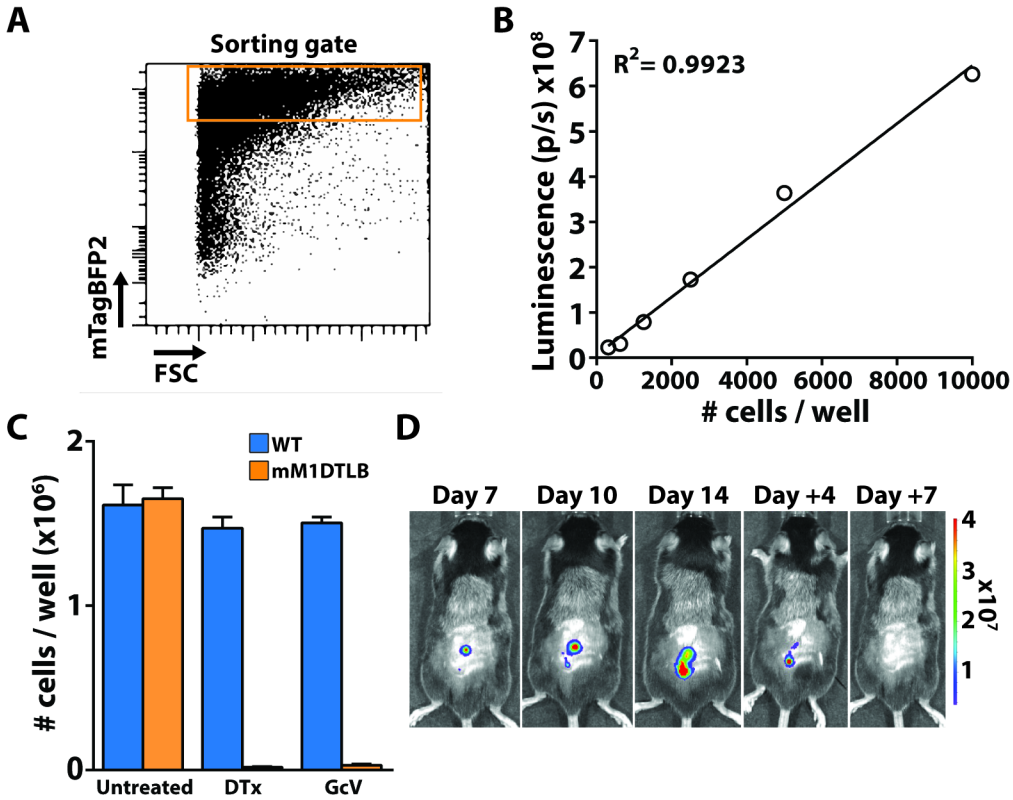

Figure S1: Validation of the mM1DTLB PDA cells. (A) Sorting gate of the mM1DTLB PDA cells (B) *In vitro* validation of luciferase activity. mM1DTLB PDA cells were plated in increasing numbers and imaged for bioluminescence. A standard curve was generated. (C) $1x10^6$ unmodified or mM1DTLB PDA cells were plated and treated overnight with DTx or GcV and the number of cells per well was counted. (D) Representative example of the pre-immunization protocol. 10^6 mM1DTLB PDA cells were subcutaneously injected and bioluminescence imaging was performed on 7, 10 and 14 days after injection. DTx and GcV were administrated day 14 and 15 and bioluminescence of the tumor elimination was performed 4 and 7 days after injection.

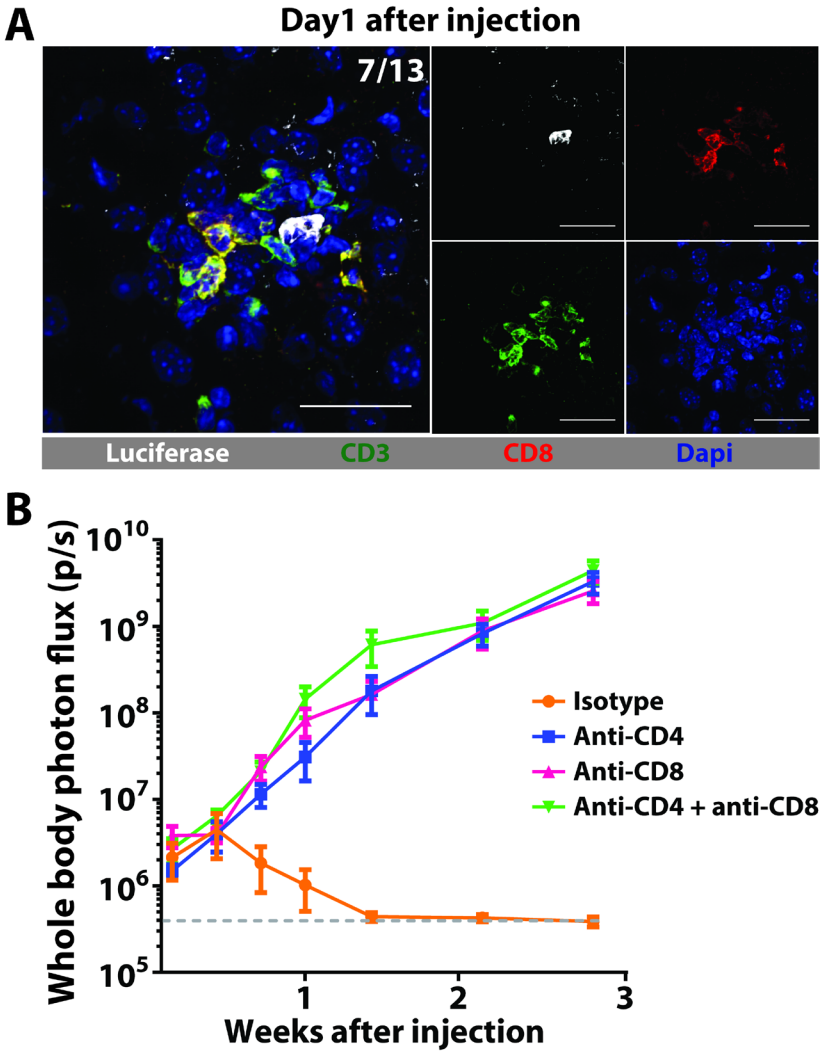

Figure S2: Prevention of metastatic growth in pre-immunized mice requires both $CD4^+$ and $CD8^+$ T cells. (A) IF of sections from the liver of a pre-immunized mouse one day after injection of mM1DTLB PDA cells that have been stained with anti-luciferase to reveal cancer cells (white), anti-CD3 (green) and anti-CD8 (red). The ratios shown in the top right corners of the photomicrographs represent the frequency of the observed DCC phenotype relative to the total number of DCCs that were assessed. All frequencies are compiled in **table S2**. Scale bar = 25μm. (B) Tumor growth was measured by bioluminescent imaging of pre-immunized mice treated with isotype control (orange), anti-CD4 (blue), anti-CD8 (pink) or a combination of the two antibodies (green), starting on the day of the injection of mM1DTLB PDA cells. n=5 mice per group. Dashed gray line represents the background luminescence in tumor-free mice.

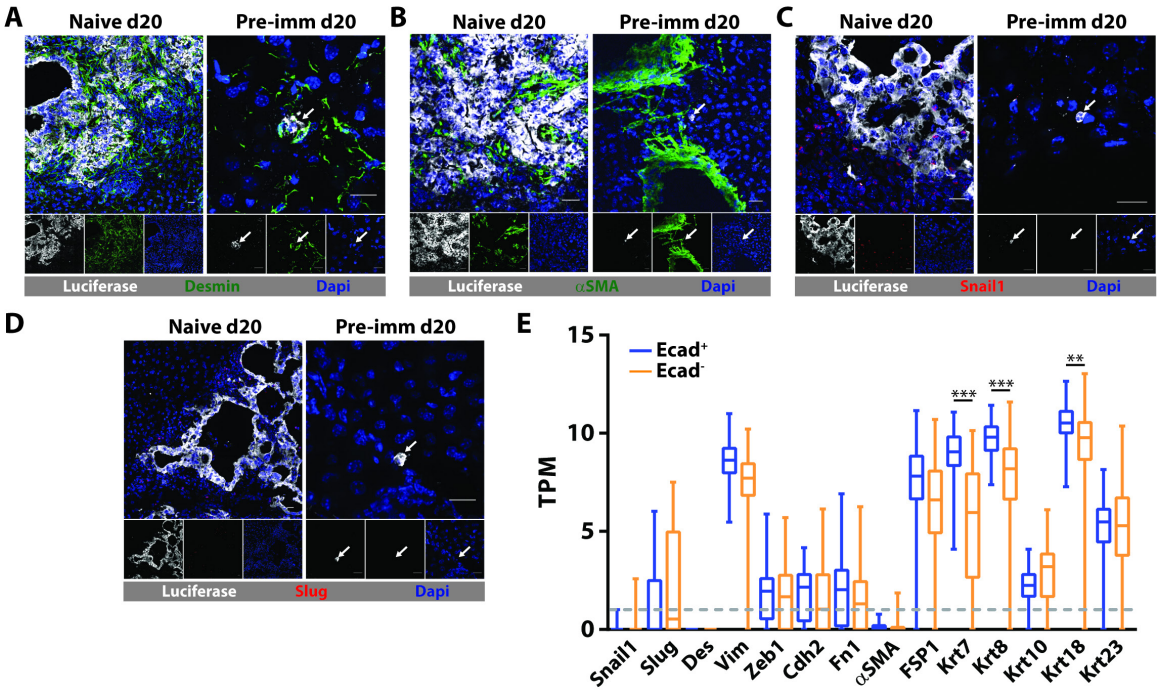

Figure S3: Absent mesenchymal markers in hepatic DCCs. (A-D) IF of sections from the livers of naïve (left panels) and pre-immunized mice (right panels) 20 days after the injection of mM1DTLB PDA cells that have been stained with anti-luciferase to reveal cancer cells (white) and (A) anti-desmin (green), (B) anti-αSMA (green), (C) anti-Snail1 (red) or anti-Slug (red). Arrows designate DCCs. Scale bar = 25μm. (E) Transcriptomic analysis by scRNAseq of mesenchymal gene expression in FACS-sorted Ecad^{+} (blue) or Ecad^{-} (orange) mM1DTLB PDA cells. Expression is given in transcripts per million (TPM) and dashed gray line represents the level above which genes are considered expressed.

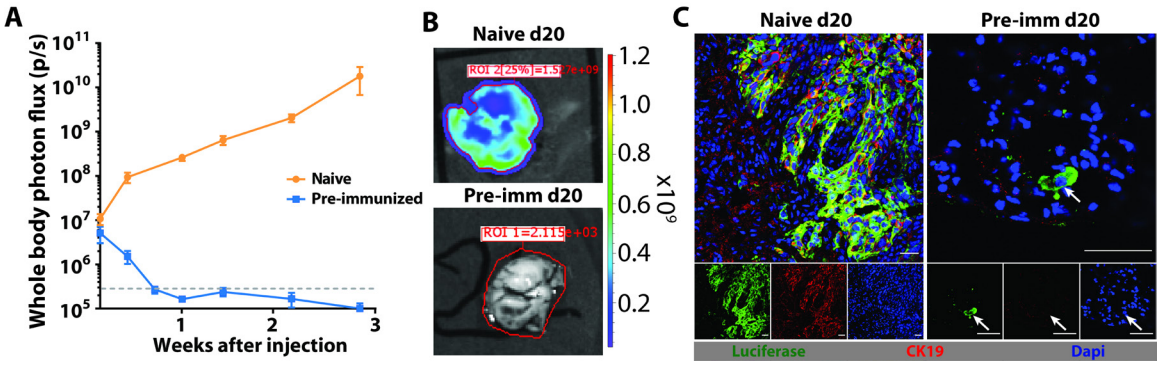

Figure S4: Model of latent pulmonary DCCs. (A) Growth of pulmonary metastases after tail vein injection of mM1DTLB cells into naïve and pre-immunized mice was assessed by whole body bioluminescent imaging. Dashed gray line represents the background luminescence in tumor-free mice. (B) Ex vivo photon flux of whole lungs was also measured at day 20 after injection of mM1DTLB PDA cells. n=5 mice per group. (C) IF of sections from the lungs of a naïve and pre-immunized mice 20 days after injection of mM1DTLB cells. Staining was performed with anti-luciferase to reveal cancer cells (green) and anti-CK19 (red). Arrows designate DCCs. Scale bar = 25μm.

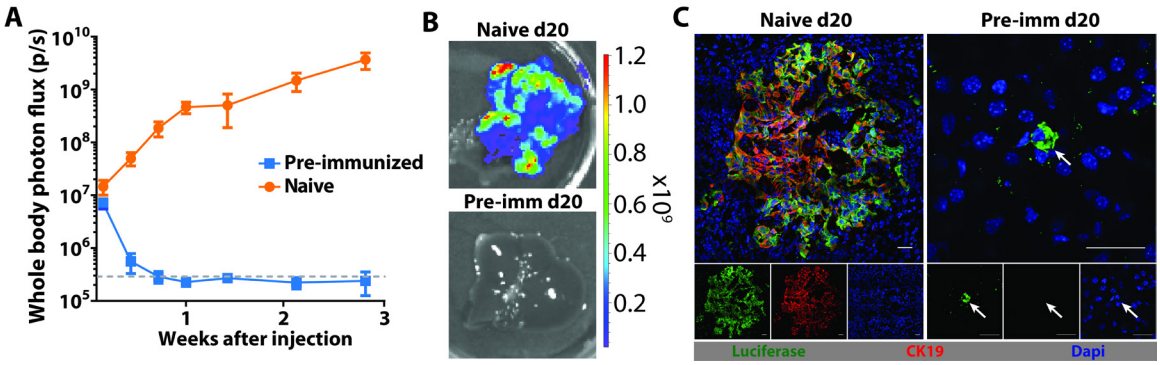

Figure S5: Model of latent hepatic DCCs formed with cancer cells derived from a primary KPC tumor. (A) Growth of hepatic metastases was measured by whole body bioluminescent imaging of naïve and pre-immunized mice after intra-splenic injection of 1242DTLB cells. Dashed gray line represents the background luminescence in tumor-free mice. (B) Ex vivo photon flux of whole livers was also measured at day 20 after injection of 1242DTLB cells. n=5 mice per group. (C) IF of sections from the liver of a naïve and pre-immunized mice 20 days after intra-splenic injection of 1242DTLB cells. Staining was performed with anti-luciferase (green) and anti-CK19 (red). Arrows designate DCCs. Scale bar = 25μm.

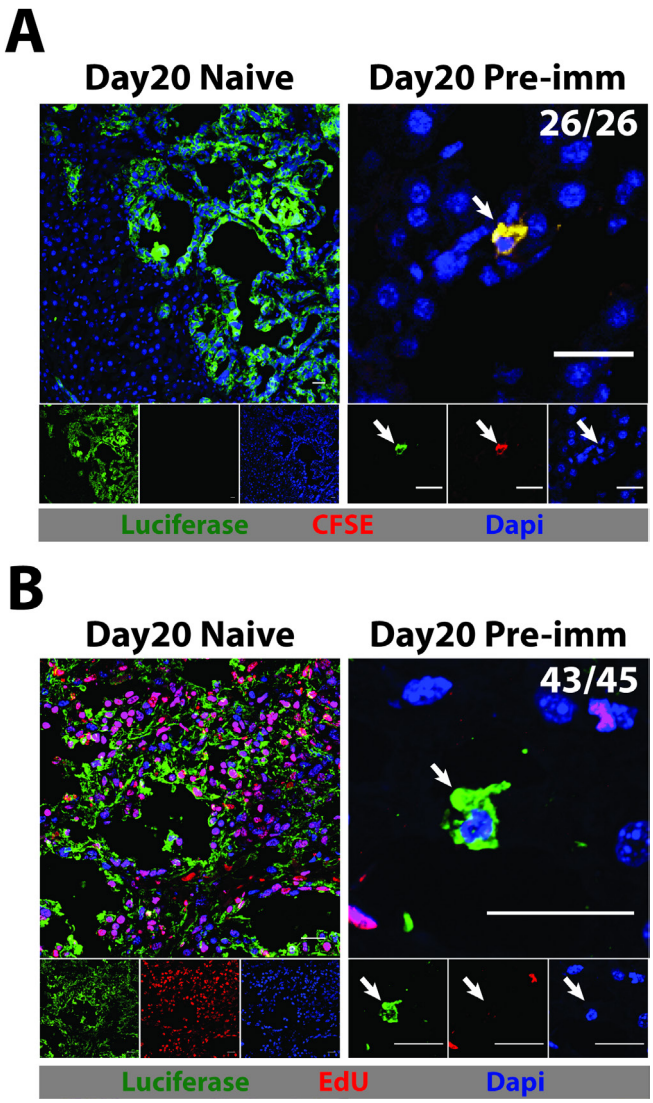

Figure S6: Non-proliferative state of hepatic DCCs. Pre-injection mM1DTLB cells were loaded with CFSE. EdU was given to the mice in the drinking water starting on the day of intra-splenic injection. (A and B) IF of sections from the livers of naïve (left panels) and pre-immunized mice (right panels) 20 days after the injection of mM1DTLB cells. Sections were stained with anti-luciferase (green) and assessed for (A) CFSE fluorescence (red) or (B) EdU incorporation (red). The ratios shown in the top right corners of the photomicrographs represent the frequency of the observed DCC phenotype relative to the total number of DCCs that were assessed. All frequencies are compiled in **table S2**. Arrows designate DCCs. Scale bar = 25μm.

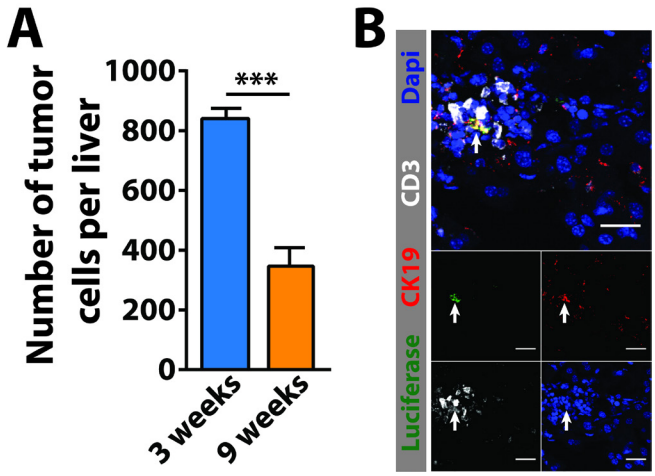

Figure S7: Spontaneous decrease of hepatic DCCs in pre-immunized mice. (A) The number of hepatic DCCs was measured 3 weeks and 9 weeks after intra-splenic injection of 10^6 mM1DTLB cells. *** = p<0.001. (B) IF of a section from the liver of a pre-immunized mouse 20 days after the injection of mM1DTLB PDA cells stained with anti-luciferase (green), anti-CK19 (red) and anti-CD3 (white) reveals a rare CK19$^+$ DCC surrounded by CD3+ T cells. Arrows designate the DCC. Scale bar = 25μm.

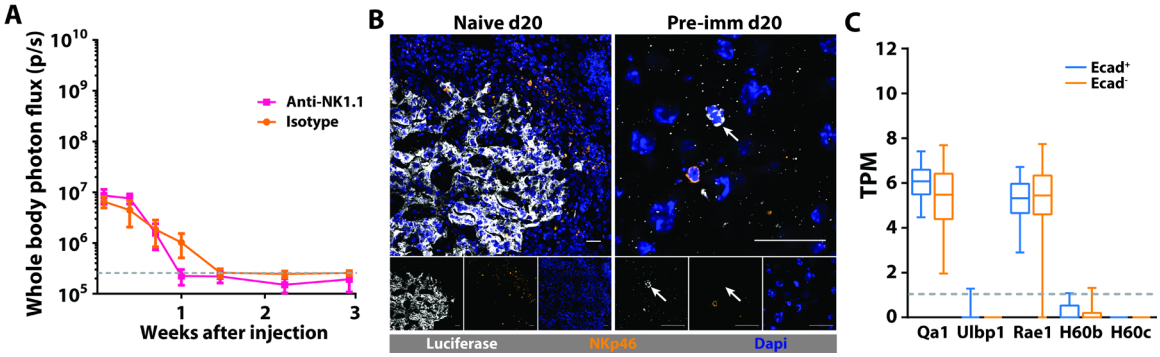

Figure S8: Absent role of NK cells in the selection of DCCs. (A) Growth of hepatic metastases was measured by whole body bioluminescent imaging of pre-immunized mice treated with isotype control (orange) or depleting anti-NK1.1 antibody (pink) from the day of intra-splenic injection of mM1DTLB cells. n=5 mice per group. Dashed gray line represents the background luminescence in tumor-free mice. (B) IF of sections from the livers of naïve (left panel) and pre-immunized mice (right panel) 20 days after the injection of mM1DTLB cells. Sections were stained with anti-luciferase (white) and anti-NKp46 for NK cells (orange). (C) Transcriptomic analysis by scRNAseq of the expression of genes encoding the major NK cell ligands by FACS-sorted Ecad$^+$ (blue) or Ecad$^-$ (orange) mM1DTLB cells. Expression is given in transcripts per million (TPM) and dashed gray line represents the level above which genes are considered expressed.

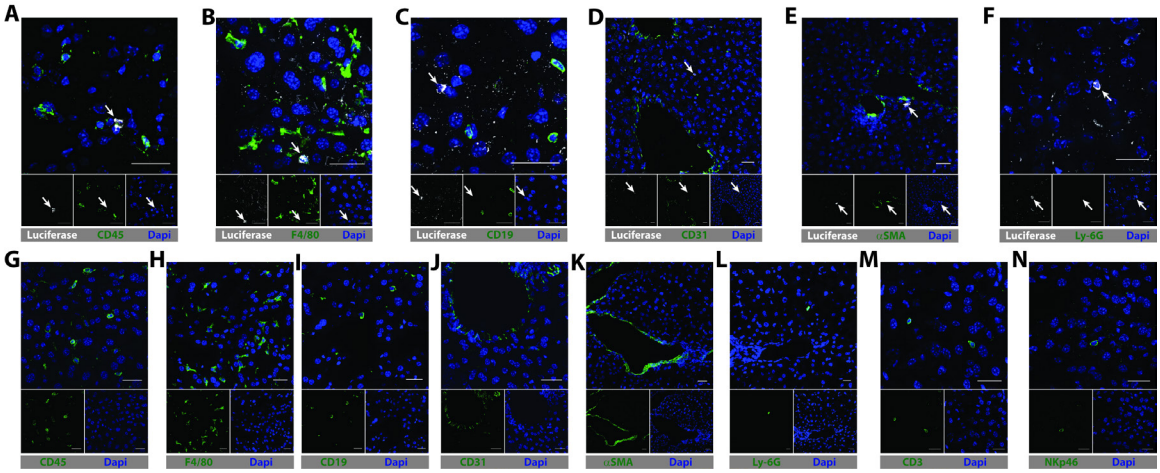

Figure S9: Absent inflammatory response near hepatic DCCs. (A-F) IF of sections from the liver of a pre-immunized mouse 20 days after intra-splenic injection of mM1DTLB cells. Sections were stained with anti-luciferase (white) and (A) anti-CD45 (green), (B) anti-F4/80 (green), (C) anti-CD19 (green), (D) anti-CD31 (green),(E) anti-αSMA (green), and (F) anti-Ly-6G (green). (G-N) IF of sections from the liver of a non-injected mouse. Sections were stained with (G) anti-CD45 (green), (H) anti-F4/80 (green), (I) anti-CD19 (green), (J) anti-CD31 (green), (K) anti-αSMA (green), (L) anti-Ly-6G (green), (M) anti-CD3 (green), and (N) anti-NKp46 (green). Arrows designate DCCs. Scale bar = 25μm.

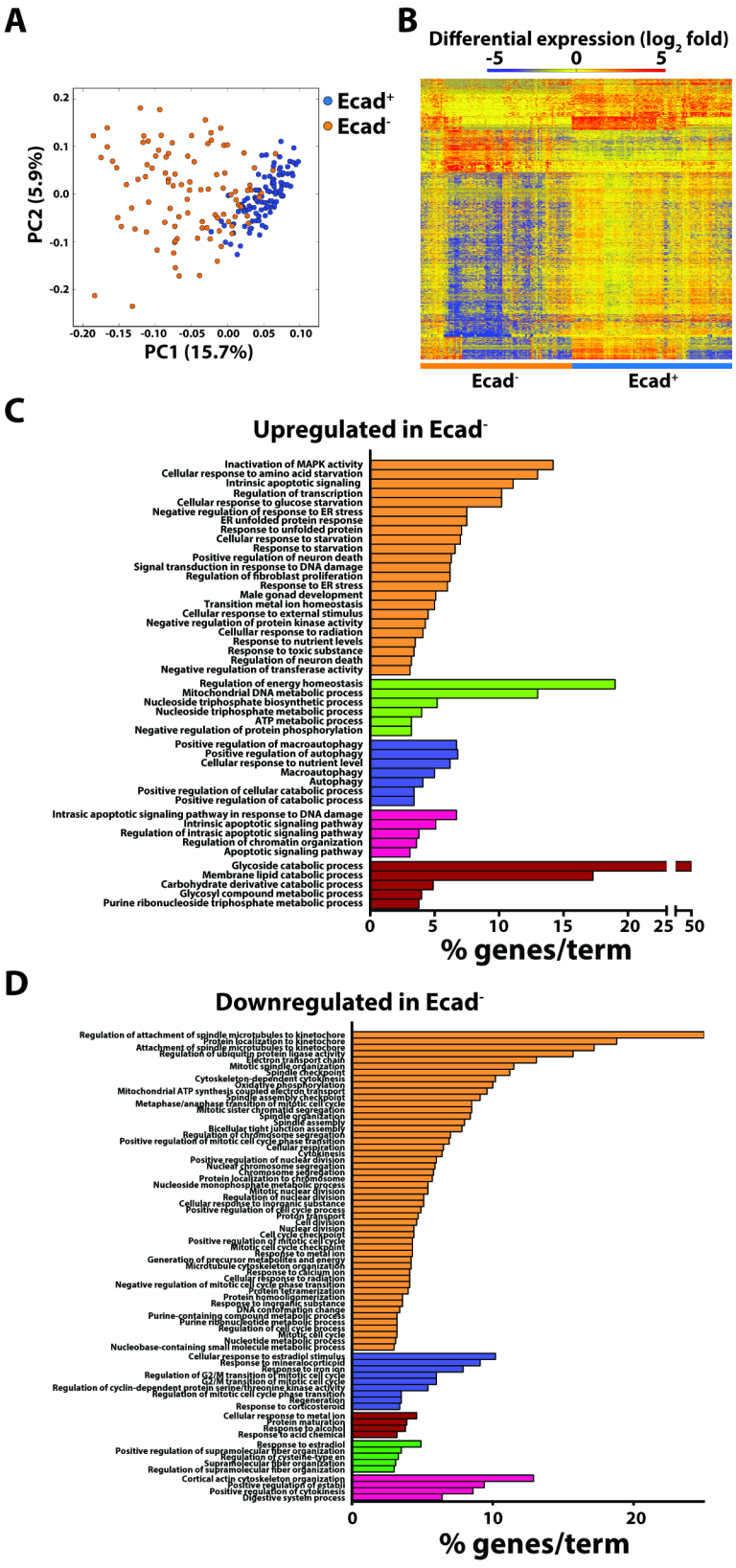
A
Ecad+
Ecad-
PC2 (5.9%)
PC1 (15.7%)
B
Differential expression (log2 fold)
-5
0
5
Ecad-
Ecad+
C
Upregulated in Ecad-
Inactivation of MAPK activity
Cellular response to amino acid starvation
Intrinsic apoptotic signaling
Regulation of transcription
Cellular response to glucose starvation
Negative regulation of response to ER stress
ER unfolded protein response
Response to unfolded protein
Cellular response to starvation
Response to starvation
Positive regulation of neuron death
Signal transduction in response to DNA damage
Regulation of fibroblast proliferation
Response to ER stress
Male gonad development
Transition metal ion homeostasis
Cellular response to external stimulus
Negative regulation of protein kinase activity
Cellular response to radiation
Response to nutrient levels
Response to toxic substance
Regulation of neuron death
Negative regulation of transferase activity
Regulation of energy homeostasis
Mitochondrial DNA metabolic process
Nucleoside triphosphate biosynthetic process
Nucleoside triphosphate metabolic process
ATP metabolic process
Negative regulation of protein phosphorylation
Positive regulation of macroautophagy
Positive regulation of autophagy
Cellular response to nutrient level
Macroautophagy
Autophagy
Positive regulation of cellular catabolic process
Positive regulation of catabolic process
Intrasic apoptotic signaling pathway in response to DNA damage
Intrinsic apoptotic signaling pathway
Regulation of intrasic apoptotic signaling pathway
Regulation of chromatin organization
Apoptotic signaling pathway
Glycoside catabolic process
Membrane lipid catabolic process
Carbohydrate derivative catabolic process
Glycosyl compound metabolic process
Purine ribonucleoside triphosphate metabolic process
% genes/term
D
Downregulated in Ecad-
Regulation of attachment of spindle microtubules to kinetochore
Protein localization to kinetochore
Attachment of spindle microtubules to kinetochore
Regulation of ubiquitin protein ligase activity
Electron transport chain
Mitotic spindle organization
Spindle checkpoint
Cytoskeleton-dependent cytokinesis
Coupled electron transport
Mitochondrial ATP synthesis
Spindle assembly checkpoint
Metaphase/anaphase transition of mitotic cell cycle
Mitotic sister chromatid segregation
Spindle organization
Spindle assembly
Bicellular tight junction assembly
Regulation of chromosome segregation
Positive regulation of mitotic cell cycle phase transition
Cellular respiration
Cytokinesis
Positive regulation of nuclear division
Nuclear chromosome segregation
Chromosome segregation
Protein localization to chromosome
Nucleoside monophosphate metabolic process
Mitotic nuclear division
Regulation of nuclear division
Cellular response to inorganic substance
Positive regulation of cell cycle process
Protein transport
Cell division
Nuclear division
Cell cycle checkpoint
Positive regulation of mitotic cell cycle
Mitotic cell cycle checkpoint
Response to metal ion
Generation of precursor metabolites and energy
Microtubule cytoskeleton organization
Response to inorganic substance
Cellular response to radiation
Negative regulation of mitotic cell cycle phase transition
Protein tetramerization
Protein homooligomerization
Response to inorganic substance
DNA conformation change
Purine-containing compound metabolic process
Purine ribonucleotide metabolic process
Regulation of cell cycle process
Mitotic cell cycle
Nucleotide metabolic process
Nucleobase-containing small molecule metabolic process
Cellular response to estradiol stimulus
Response to mineralocorticoid
Response to iron ion
Regulation of G2/M transition of mitotic cell cycle
G2/M transition of mitotic cell cycle
Regulation of cyclin-dependent protein serine/threonine kinase activity
Regulation of mitotic cell cycle phase transition
Gluconeogenesis
Response to corticosteroid
Cellular response to metal ion
Protein maturation
Response to alcohol
Response to acid chemical
Response to estradiol
Positive regulation of supramolecular fiber organization
Regulation of cysteine-type en
Supramolecular fiber organization
Regulation of supramolecular fiber organization
Cortical actin cytoskeleton organization
Positive regulation of establi
Positive regulation of cytokinesis
Digestive system process
% genes/term

Figure S10: Additional analyses of the scRNAseq of mM1DTLB cells. FASC-sorted Ecad^{+} and Ecad^{-} mM1DTLB PDA cells were processed on a Fluidigm C1 platform and subjected to scRNA-Seq. (A) The single cell transcriptomes of 104 Ecad^{+} and 98 Ecad^{-} were analyzed by PCA, (B) and a heatmap of the 1639 differentially expressed genes between Ecad^{+} and Ecad^{-} cells with at least a two-fold differential expression was generated. (C-D) The GO biological terms relating to each of the nodes that are depicted in in Fig.4, showing the proportion of genes changed per term in (C) upregulated pathways and (D) downregulated pathways in Ecad^{-} cells, respectively.

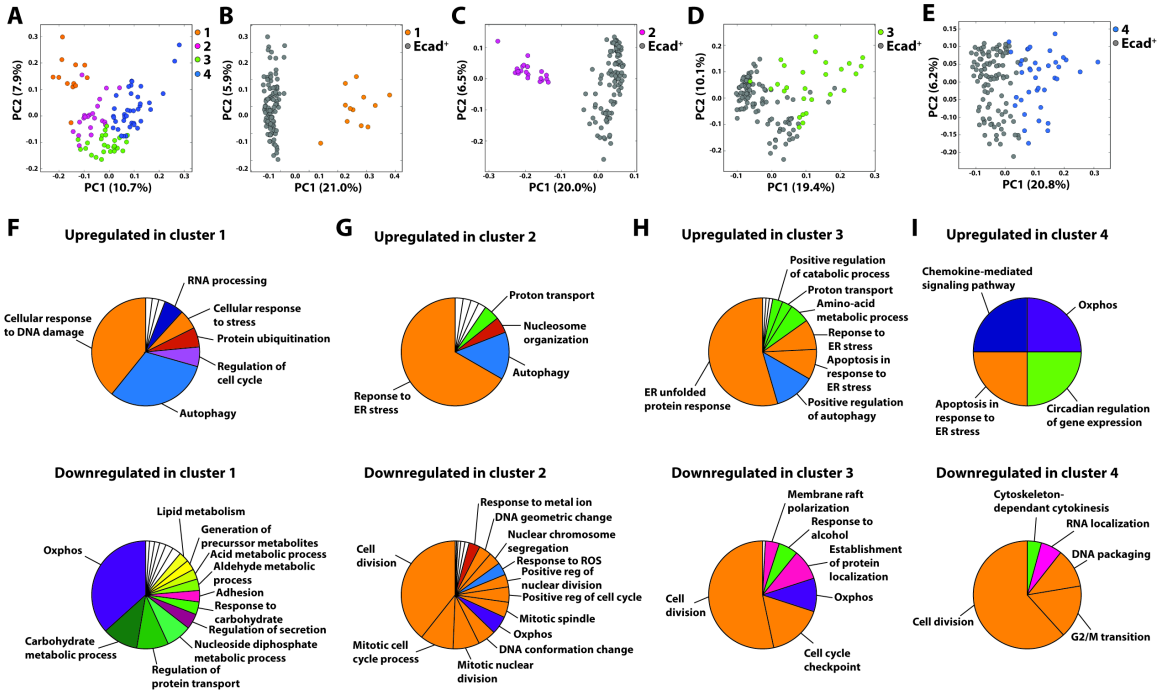

Figure S11: Analyses of single Ecad^{-} cell diversity by scRNAseq. The 98 sequenced Ecad^{-} mM1DTLB PDA cells were subjected to (A) unsupervised PCA, identifying a diversity of four clusters. (B-E) The transcriptomes of each of the four clusters were compared by PCA with the 104 Ecad^{+} mM1DTLB PDA cells and subjected to pathway enrichment analysis. The relative representation of pathways is depicted as pie charts for upregulated pathways (top panels) and downregulated pathways (bottom panels) in (F) cluster 1, (G) cluster 2, (H) cluster 3 and (I) cluster 4 compared to Ecad^{+} mM1DTLB PDA cells. The depicted pathways are significant with an adjusted $p<0.01$ after Benjamini-Hochberg false discovery rate.

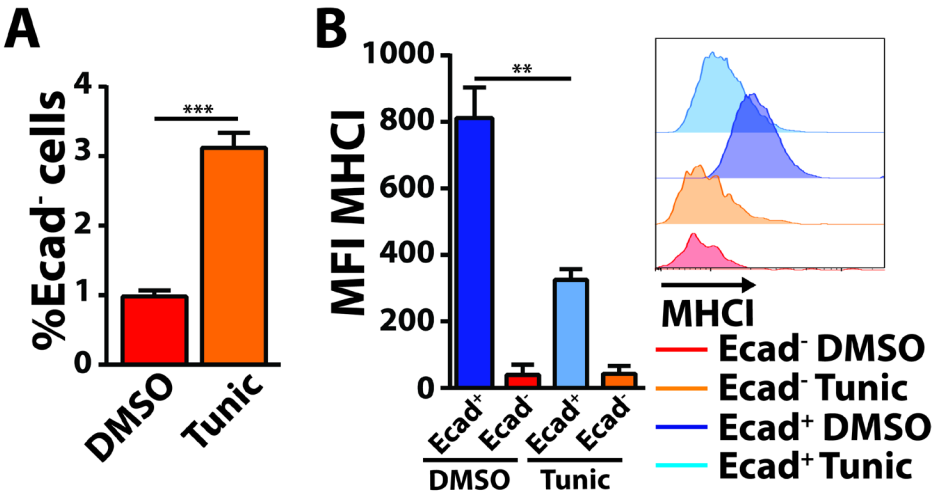

Figure S12: Stimulation of the ER stress response with tunicamycin *in vitro* and the DCC phenotype . mM1DTLB PDA cells were treated for 14 h with tunicamycin (Tunic), or DMSO. (A) The proportion of PDA cells that did nor did not express Ecad, (B) and the MFI of MHCI expression by the different PDA populations was measured by flow cytometry. Data are representative of three independent experiments. ** = p<0.01, *** = p<0.001.

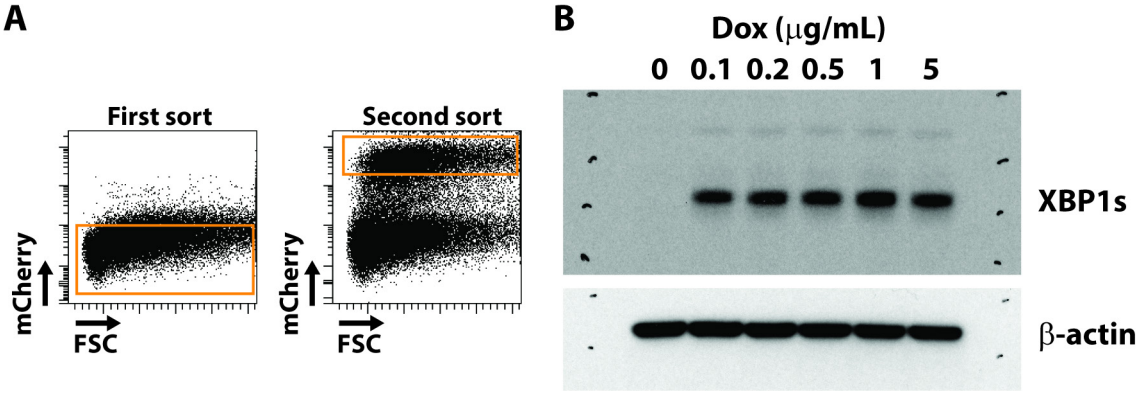

Figure S13: Validation of inducible expression of XBP1s by Dox-treated mM1TetXBP1s PDA cells. (A) Sorting gates for the selection of mM1TetXBP1s PDA cells. (B) Western blot validation of inducible XBP1s. Cells were seeded in 6 well plate with or without Dox at indicated concentration. 30 h after treatment, cells were lysed in RIPA buffer with protease and phosphatase inhibitors. Protein concentration was estimated by Bradford. 20μg protein was loaded on a 4-12% gel. The blot was probed with the XBP1s antibody and then stripped and re-probed with the β-actin antibody.

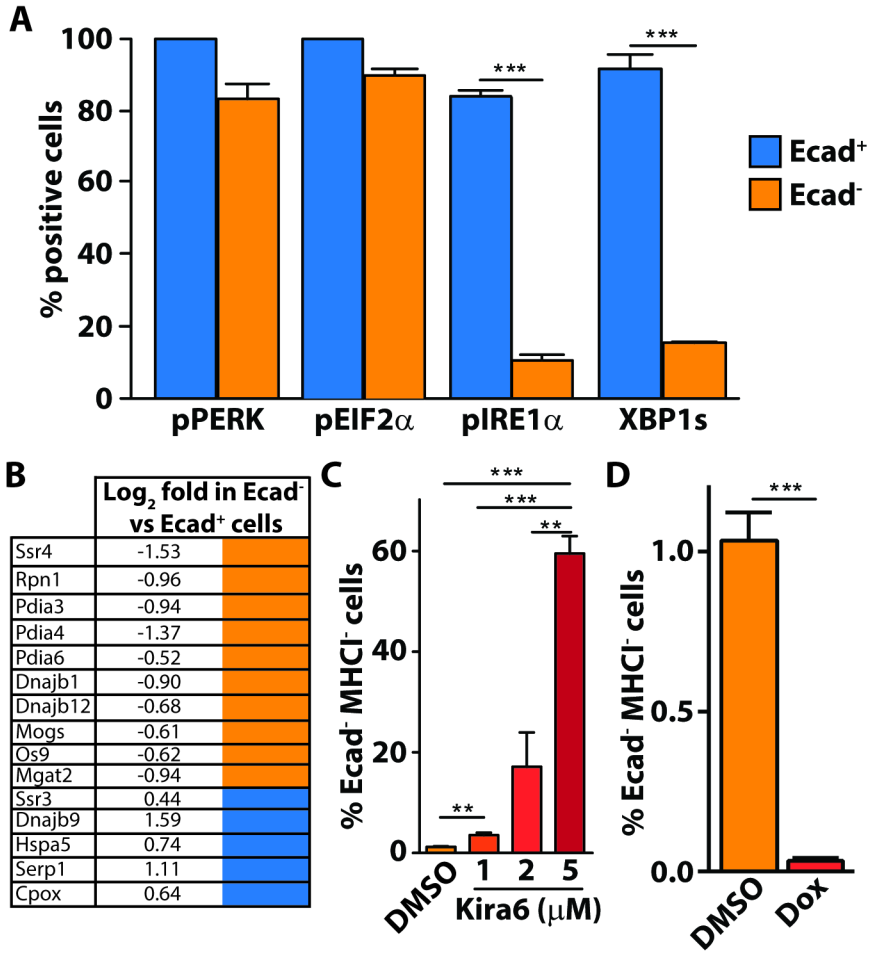

Figure S14: Analysis of the unfolded protein response pathways in PDA cells in vitro. (A) Flow cytometry analysis of Ecad$^+$ and Ecad$^-$ mM1DTLB PDA cells for the phosphorylated forms of PERK, EIF2α and IRE1α, and the expression of XBP1s. (B) Transcriptomic analysis by scRNAseq of XBP1 target genes downregulated or upregulated in Ecad$^-$ mM1DTLB PDA cells relative to Ecad+ cells. (C) The proportion of Ecad$^-$ MHCI$^-$ mM1DTLB PDA cells was determined by flow cytometry after treatment for 14 h with increasing doses of the Kira6 inhibitor of IRE1α kinase activity. (D) The proportion of mM1TetXBP1s PDA cells that are Ecad$^-$ MHCI$^-$ was determined by flow cytometry after treatment for 14 h with Dox.

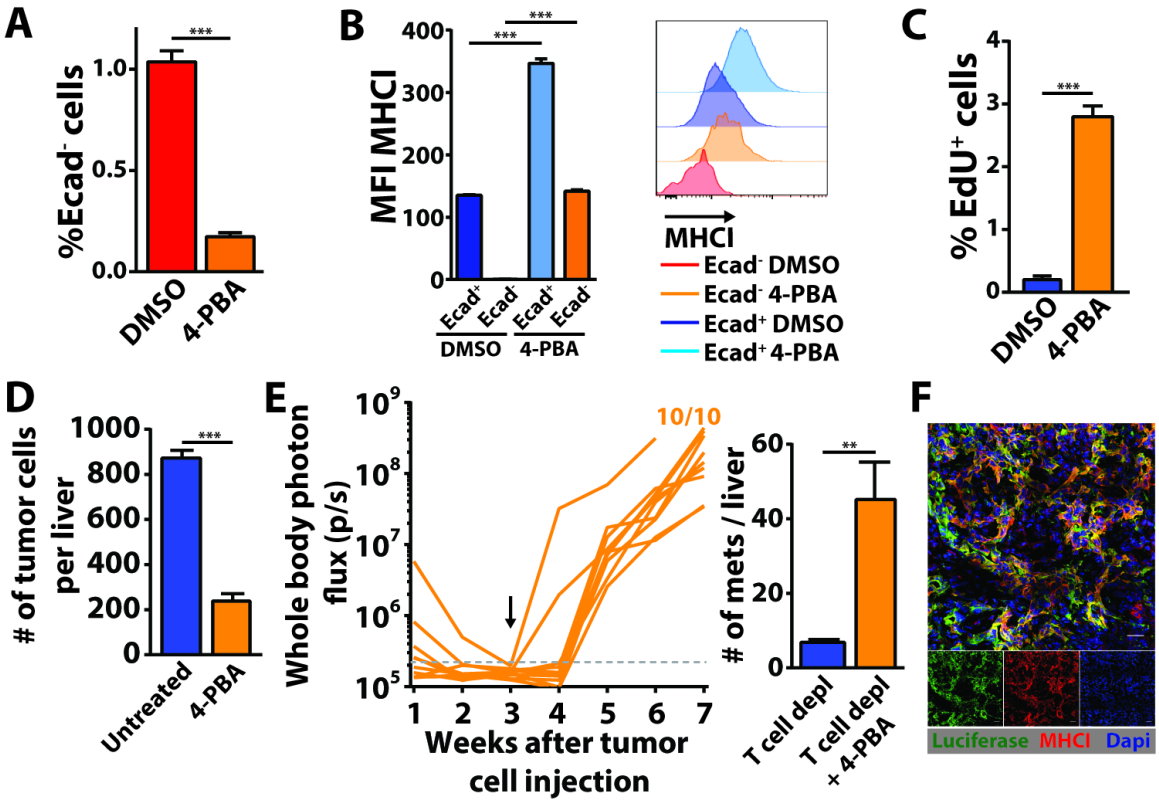

Figure S15: The effects on DCCs of relieving ER stress with the 4-PBA chemical chaperone. (A and B) mM1DTLB PDA cells were treated for 14 h with 4-PBA or DMSO. (A) The proportion of PDA cells that were Ecad$^-$, (B) and the MFI of MHCI expression were measured by flow cytometry. Data are representative of three independent experiments (STATS?). (C) mM1DTLB PDA cells were treated with 100μm GcV for two days and the remaining, non-cycling cells were pulsed overnight with EdU duruing culture in the presence or absence of 4-PBA. The proportion of EdU$^+$ cells was assessed by flow cytometry. (D) Pre-immunized mice (n=5) that had received splenic injections of mM1DTLB PDA cells were treated with 4-PBA from the day of the injection. The number of hepatic DCCs was quantified after three weeks and compared to that of mice not receiving 4-PBA (n=5). (E) Pre-immunized mice that had received splenic injections of mM1DTLB PDA cells were treated with 4-PBA beginning three weeks later. T cells were depleted by administering anti-CD4 and anti-CD8 antibodies. Growth of hepatic metastases was assessed by whole body bioluminescent imaging (left panel), and the number of metastases was determined by by bioluminescence of the resected livers (right panel). n=10 mice. ** = $p<0.01$, *** = $p<0.001$. (F) IF of sections from a liver taken from a pre-immunized mouse that had been treated with 4-PBA and depleted of T cells starting three weeks after intra-splenic injection of mM1DTLB PDA cells. The sections were stained with anti-luciferase (green) and anti-MHCI (red). Arrows designate DCCs. Scale bar = 25μm.